Large Displacement Analysis of Naturally Curved and Twisted Composite Beams

O. A. Bauchau* and C. H. Hong†
Rensselaer Polytechnic Institute, Troy, New York

This paper presents an efficient procedure for analyzing naturally curved and twisted beams undergoing large displacements and rotations but small strains. Special care is taken to accurately model the structural behavior of the beam: shearing deformations as well as torsion-related warping are taken into account. The various elastic couplings (e.g., bending-twisting or extention-twisting) that can arise in composite beams are also modeled in a rational fashion. The equations are derived in curvilinear material coordinates, and Euler angles are used to represent the arbitrarily large rotations. The strain energy in the beam is reduced to a quadratic expression by means of a quasilinearization procedure. This expression of the strain energy is the basis for a finite-element analysis of the structure, and standard iteration techniques are used to obtain nonlinear solutions to the problem. The predictions of this model are found to be in good agreement with the experimental results, and the computational efficiency is greatly improved as compared with other available analyses.

Introduction

STATIC and dynamic nonlinear analysis of naturally curved and twisted beams has many important applications in mechanical and aeronautical engineering. Helicopter blades and flexible space structures are specific cases that have received considerable attention in recent years.[1-3] The nonlinear kinematics involved in the problem are complex because in three-dimensional analysis, large rotations that are not vector quantities have to be accounted for. In addition, when composite materials are used several nonclassical effects become important, such as transverse shear deformations and torsion-related warpings. Elastic couplings, e.g., bending-twisting and/or extension-twisting couplings, are also possible and should be included in the analysis.

Three-dimensional beam elements have been developed[4] and used in several engineering applications.[5,6] This procedure allows the modeling of very general configurations, including naturally curved and twisted beams. However, numerical integration must be performed over the cross section of the beam at each Gaussian station along the axis, resulting in a high computational cost. In most analyses, an incremental approach is employed, and at each step the linearized equations involve small rotations only, slowing down the convergence rate of the algorithm.

The objective of this paper is to present a consistent, nonlinear analysis of naturally curved and twisted beams, with special attention devoted to the modeling of composite beams and greater numerical efficiency. Both static and dynamic analyses have been implemented and several examples are presented.

Geometry Before Deformation

The axis of the beam is represented by a continuous curve in space, given in a parametric form $\boldsymbol{r}_0(s)$ where s is the curvilinear coordinate along the axis (see Fig. 1). The tangent unit vector to this curve is λ. Two mutually orthogonal unit vectors $\boldsymbol{i}_\xi$ and $\boldsymbol{i}_\eta$ define the plane of the cross section of the beam, so that at each point along the axis, λ, $\boldsymbol{i}_\xi$, $\boldsymbol{i}_\eta$ form an orthonormal triad. The derivatives of these vectors are

$$\begin{bmatrix} \lambda' \\ \boldsymbol{i}_\xi' \\ \boldsymbol{i}_\eta' \end{bmatrix} = \begin{bmatrix} 0 & \kappa_\eta & -\kappa_\xi \\ -\kappa_\eta & 0 & \kappa_s \\ \kappa_\xi & -\kappa_s & 0 \end{bmatrix} \begin{bmatrix} \lambda \\ \boldsymbol{i}_\xi \\ \boldsymbol{i}_\eta \end{bmatrix} \tag{1}$$

where the primes denote derivatives with respect to s. The twist of the beam is κ_s, whereas κ_ξ and κ_η are the curvatures. The position vector $\boldsymbol{r}$ of an arbitrary point $\boldsymbol{P}$ of the beam can be written as

$$\boldsymbol{r}(s,\xi,\eta) = \boldsymbol{r}_0(s) + \xi \boldsymbol{i}_\xi(s) + \eta \boldsymbol{i}_\eta(s) \tag{2}$$

where the coordinates s,ξ,η appear as a natural set of curvilinear coordinates to describe the beam. Whenever convenient, the notation $(\alpha^1,\alpha^2,\alpha^3)$ will be used instead of (s,ξ,η). The base vectors[7,8] of this curvilinear coordinate system are

$$\boldsymbol{g}_i = \frac{\partial \boldsymbol{r}}{\partial \alpha^i} \tag{3}$$

the metric tensor is

$$g_{ij} = \boldsymbol{g}_i \cdot \boldsymbol{g}_j \tag{4}$$

and its determinant

$$g = (1 - \xi\kappa_\eta + \eta\kappa_\xi)^2 \tag{5}$$

Finally, we introduce a local rectangular Cartesian coordinate system y^1, y^2, y^3 that has its origin on the axis of the beam, and its unit vectors $\boldsymbol{j}^1$, $\boldsymbol{j}^2$, $\boldsymbol{j}^3$ are in the direction of λ, $\boldsymbol{i}_\xi$, and $\boldsymbol{i}_\eta$, respectively. The relation between these two coordinate systems is governed by

$$\frac{\partial y^i}{\partial \alpha^j} = \begin{bmatrix} \sqrt{g} & 0 & 0 \\ -\eta\kappa_s & 1 & 0 \\ \xi\kappa_s & 0 & 1 \end{bmatrix} \tag{6}$$

Strain Analysis

The position vector of a point $\boldsymbol{P}$ after deformation is denoted by $\boldsymbol{R}$ and the displacement vector is

$$\boldsymbol{u}(s,\xi,\eta) = \boldsymbol{R}(s,\xi,\eta) - \boldsymbol{r}(s,\xi,\eta) \tag{7}$$

Received May 19, 1986.

*Assistant Professor, Department of Mechanical Engineering, Aeronautical Engineering and Mechanics.

†Graduate Assistant, Department of Mechanical Engineering, Aeronautical Engineering and Mechanics.

The first assumption in this development is to write the displacement field in the following form:[9]

$$u(s,\xi,\eta) = [u(s) + \xi\theta_1(s) + \eta\theta_2(s)]\boldsymbol{\lambda} + [v(s) + \xi\psi_1(s) + \eta\psi_2(s)]\boldsymbol{i}_\xi + [w(s) + \xi\chi_1(s) + \eta\chi_2(s)]\boldsymbol{i}_\eta \tag{8}$$

The base vectors in the deformed configuration are

$$\boldsymbol{G}_i = \frac{\partial \boldsymbol{R}}{\partial \alpha^i} \tag{9}$$

Combining Eqs. (3), (7), and (8) yields

$$\begin{aligned}
\boldsymbol{G}_1 &= (\sqrt{g} + \epsilon_s + \xi\lambda_s + \eta\nu_s)\boldsymbol{\lambda} + (-\eta\kappa_s + \epsilon_\xi + \xi\lambda_\xi + \eta\nu_\xi)\boldsymbol{i}_\xi + (\xi\kappa_s + \epsilon_\eta + \xi\lambda_\eta + \eta\nu_\eta)\boldsymbol{i}_\eta \\
\boldsymbol{G}_2 &= \theta_1\boldsymbol{\lambda} + (1+\psi_1)\boldsymbol{i}_s + \chi_1\boldsymbol{i}_\eta \\
\boldsymbol{G}_3 &= \theta_2\boldsymbol{\lambda} + \psi_2\boldsymbol{i}_\xi + (1+\chi_2)\boldsymbol{i}_\eta
\end{aligned} \tag{10}$$

where

$$\left|\begin{aligned}
\xi_s &= u' - \kappa_\eta v + \kappa_\xi w \\
\epsilon_\xi &= v' - \kappa_s w + \kappa_\eta u \\
\epsilon_\eta &= w' - \kappa_\xi u + \kappa_s v
\end{aligned}\right. \tag{11}$$

$$\left|\begin{aligned}
\lambda_s &= \theta_1' - \kappa_\eta\psi_1 + \kappa_\xi\chi_1 \\
\lambda_\xi &= \psi_1' - \kappa_s\chi_1 + \kappa_\eta\theta_1 \\
\lambda_\eta &= \chi_1' - \kappa_\xi\theta_1 + \kappa_s\psi_1
\end{aligned}\right. \tag{12}$$

$$\left|\begin{aligned}
\nu_s &= \theta_2' - \kappa_\eta\psi_2 + \kappa_\xi\chi_2 \\
\nu_\xi &= \psi_2' - \kappa_s\chi_2 + \kappa_\eta\theta_2 \\
\nu_\eta &= \chi_2' - \kappa_\xi\theta_2 + \kappa_s\psi_2
\end{aligned}\right. \tag{13}$$

The Green-Lagrange strains f_{ij} in the curvilinear coordinate system[7] are

$$f_{ij} = \tfrac{1}{2}(G_{ij} - g_{ij}) \tag{14}$$

where $G_{ij} = \boldsymbol{G}_i$. In the deformed configuration, $\boldsymbol{G}_j$ is the metric tensor. Finally, the strains e_{ij} in the local rectangular coordinate system are obtained from

$$e_{ij} = \frac{\partial\alpha^k}{\partial y^i}\frac{\partial\alpha^\ell}{\partial y^j} f_{k\ell} \tag{15}$$

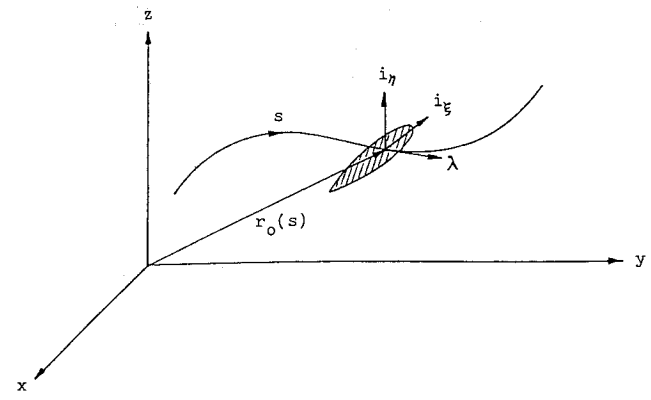

Fig. 1 Geometry of the beam.

The second assumption is that the cross section of the beam does not deform in its own plane, implying the vanishing of the strain components acting in the plane of the cross section,

$$\begin{aligned}
e_{22} &= \theta_1^2 + (1+\psi_1)^2 + \chi_1^2 - 1 = 0 \\
e_{33} &= \theta_2^2 + \psi_2^2 + (1+\chi_2)^2 - 1 = 0 \\
e_{23} &= \theta_1\theta_2 + (1+\psi_1)\psi_2 + \chi_1(1+\chi_2) = 0
\end{aligned} \tag{16}$$

These relations express the fact that only three of the six quantities θ_1, θ_2, ψ_1, ψ_2, χ_1, and χ_2 are independent quantities. Hence it is convenient to introduce the Euler angles α, β, and γ as defined in Fig. 2, yielding

$$\begin{aligned}
\theta_1 &= -C_\alpha S_\beta C_\gamma - S_\alpha S_\gamma, & \theta_2 &= C_\alpha S_\beta S_\gamma - S_\alpha C_\gamma \\
1+\psi_1 &= C_\beta C_\gamma, & \psi_2 &= -C_\beta S_\gamma \\
\chi_1 &= -S_\alpha S_\beta C_\gamma + C_\alpha S_\gamma, & 1+\chi_2 &= S_\alpha S_\beta S_\gamma + C_\alpha C_\gamma
\end{aligned} \tag{17}$$

where the notation $C_\alpha = \cos(\alpha)$, $S_\alpha = \sin(\alpha)$ etc. was used. Equations (16) are now automatically satisfied. Combining Eqs. (15), (14), and (10), the nonvanishing strain components become

$$2\sqrt{g}e_{12} = \hat{e}_{12} + \eta\kappa_{12} \tag{18}$$

$$2\sqrt{g}e_{13} = \hat{e}_{13} - \xi\kappa_{12} \tag{19}$$

$$\sqrt{g}e_{11} = \hat{e}_{11} + \xi\kappa_{11} + \eta\kappa_{22} \tag{20}$$

where

$$\begin{aligned}
\hat{e}_{11} &= \tfrac{1}{2}[(1+\epsilon_s)^2 + \epsilon_\xi^2 + \epsilon_\eta^2 - 1] \\
\hat{e}_{12} &= (1+\epsilon_s)\theta_1 + \epsilon_\xi(1+\psi_1) + \epsilon_\eta\chi_1 \\
\hat{e}_{13} &= (1+\epsilon_s)\theta_2 + \epsilon_\xi\psi_2 + \epsilon_\eta(1+\chi_2)
\end{aligned} \tag{21}$$

$$\begin{aligned}
\kappa_{11} &= (1+\epsilon_s)\omega_s + \epsilon_\xi\omega_\xi + \epsilon_\eta\omega_\eta \\
\kappa_{22} &= (1+\epsilon_s)\sigma_s + \epsilon_\xi\sigma_\xi + \epsilon_\eta\sigma_\eta \\
\kappa_{12} &= \theta_1\theta_1' + (1+\psi_1)\psi_2' + \chi_1\chi_2' - \kappa_s[\psi_1 + \chi_2 + \psi_1\chi_2 - \chi_1\psi_2] \\
&\quad + \kappa_\xi[\theta_1(1+\chi_2) - \theta_2\chi_1] + \kappa_\eta[(1+\psi_1)\theta_2 - \theta_1\psi_2]
\end{aligned} \tag{22}$$

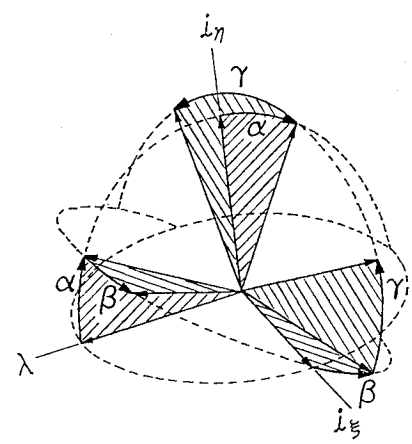

Fig. 2 Definition of the Euler angles.

and

$$\begin{aligned} \omega_s &= \theta_1' - \kappa_s\theta_2 + \kappa_\xi\chi_1 - \kappa_\eta\psi_1 & \sigma_s &= \theta_2' + \kappa_s\theta_1 + \kappa_\xi\chi_2 - \kappa_\eta\psi_2 \\ \omega_\xi &= \psi_1' - \kappa_s\psi_2 - \kappa_s\chi_1 + \kappa_\eta\theta_1 & \sigma_\xi &= \psi_2' + \kappa_s\psi_1 - \kappa_s\chi_2 + \kappa_\eta\theta_2 \\ \omega_\eta &= \chi_1' - \kappa_s\chi_2 + \kappa_s\psi_1 - \kappa_\xi\theta_1 & \sigma_\eta &= \chi_2' + \kappa_s\chi_1 + \kappa_s\psi_2 - \kappa_\xi\theta_2 \end{aligned} \tag{23}$$

In the derivation of the axial strain component e_{11}, terms in ξ^2, η^2, and $\xi\eta$ will appear. These additional terms, however, are of the same order as the squares of strain quantities.[9] The third assumption is to restrict this derivation to a small strain analysis, in which case squares of strain terms can be neglected in comparison to strain terms, reducing the axial strain expression to Eq. (20).

At this point we will focus on thin-walled beam constructions. This is not a restrictive assumption, as the present methodology could be applied to solid cross sections as well. Figure 3 depicts a typical cross section, where ζ is the curvilinear coordinate describing the contour of the section, noted C. For thin-walled beams the strain components are uniform through the wall thickness, and the only nonzero strain components are the axial strain e and the (engineering) shear strain γ,

$$e = e_{11}, \qquad \gamma = 2e_{12}\frac{d\xi}{d\zeta} + 2e_{13}\frac{d\eta}{d\zeta} \tag{24}$$

A distinguishing feature of thin-walled composite beams is their sensitivity to transverse shear and warping deformations. When the beam is subjected to transverse shear without torsion, the shearing strain distribution obtained from Eqs. (24), (18), and (19) is

$$\gamma = \frac{d\xi}{d\zeta}\hat{e}_{12} + \frac{d\eta}{d\zeta}\hat{e}_{13} \tag{25}$$

This is a very poor representation, corresponding to a "Bernoulli type" of solution.[10] A much better approximation is the St. Venant theory, where

$$\gamma = G_\xi\hat{e}_{12} + G_\eta\hat{e}_{13} \tag{26}$$

The shear strain distributions G_ξ and G_η can be obtained for arbitrary multicellular sections.[10] The torsional behavior of thin-walled composite beams is very sensitive to out-of-plane warping of the cross section. Two approaches to the modeling of this behavior were described in Ref. 11 and found to be in good agreement with experimental measurements. One of these approaches uses the St. Venant torsional warping function $\phi(\zeta)$ and is adopted in this work. The derivation of $\phi(\zeta)$ for multicellular sections was reported in Ref. 10. Since warping displacements are very small, it is not necessary to modify the kinematics of the problem. However, warping-induced strains must be added to the previously obtained strain expressions.[8,9] The final strain-displacement relationships are

$$e = \hat{e}_{11} + \xi\kappa_{11} + \eta\kappa_{22} + \phi\delta' + \tilde{\phi}\delta$$
$$\gamma = G_\xi\hat{e}_{12} + G_\eta\hat{e}_{13} - r\kappa_{12} + \tilde{\phi}\delta \tag{27}$$

where r is the distance to the tangent to the cross-sectional curve (see Fig. 3),

$$\tilde{\phi} = \kappa_s\left(\eta\frac{d\phi}{d\xi} - \xi\frac{d\phi}{d\eta}\right)$$

$$\tilde{\phi} = \frac{d\phi}{d\zeta} - \kappa_\xi\phi\frac{d\eta}{d\zeta} + \kappa_\eta\phi\frac{d\xi}{d\zeta} \tag{28}$$

and δ is a generalized coordinate for warping.

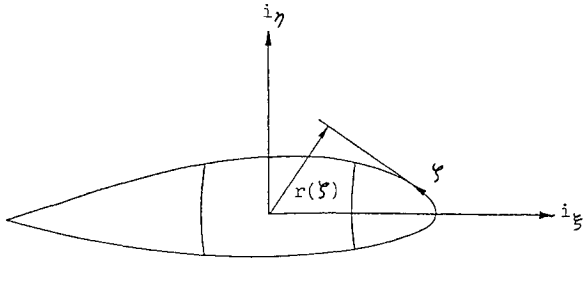

Fig. 3 Geometry of the cross section.

Strain Energy in the Beam

The principle of virtual work for the present problem[7] is

$$\int_0^L\int_S \sigma^{ij}\delta e_{ij}\sqrt{g}\,d\xi\,d\eta\,ds - \delta W = 0 \tag{29}$$

where σ^{ij} is the stress tensor in the local rectangular coordinate system, δW the virtual work done by the applied loads, S the cross-sectional area of the beam, and L its length. For a thin-walled section it reduces to

$$\int_0^L\int_C (n\delta e + q\delta\gamma)\sqrt{g}\,d\zeta\,ds - \delta W = 0 \tag{30}$$

where n and q are the axial stress flow and the shear stress flow respectively. The constitutive relationships for a thin-walled beam made of laminated composites are[10]

$$\begin{bmatrix} n \\ q \end{bmatrix} = \begin{bmatrix} A_{nn} & A_{nq} \\ A_{nq} & A_{qq} \end{bmatrix}\begin{bmatrix} e \\ \gamma \end{bmatrix} \tag{31}$$

A nonvanishing A_{nq} corresponds to the in-plane extension-shearing coupling of the laminate and results in elastic coupling for the beam. In Ref. 11 an experimental program is described that validates this modeling procedure for elastic couplings: measured twist and strain distributions were compared with theoretical predictions for thin-walled Graphite/Epoxy beams under torque. Specimens presenting elastic couplings were tested along with specimens without couplings: in both cases close agreement was found between theory and experiments. The last assumption to be made in this derivation is that the initial curvatures of the blade are moderate, to assure that

$$\sqrt{g} \approx 1 \tag{32}$$

This assumption is realistic for most practical applications, hence it does not seriously restrict the applicability of this model. The virtual work is now

$$\delta\left\{\frac{1}{2}\int_0^L\int_C (A_{nn}e^2 + A_{qq}\gamma^2 + 2A_{nq}e\gamma)\,d\zeta\,ds - W\right\} = 0 \tag{33}$$

Introducing Eq. (27) into this expression and integrating over the contour C yields

$$\delta\left\{\frac{1}{2}\int_0^L \epsilon^T H\epsilon\,ds - W\right\} = 0 \tag{34}$$

where the terms of the stiffness matrix H are listed in the Appendix and the strain vector ϵ is

$$\epsilon^T = (\hat{e}_{11}, \hat{e}_{12}, \hat{e}_{13}, \kappa_{11}, \kappa_{22}, \kappa_{12}, \delta, \delta') \tag{35}$$

In this formulation, seven independent functions describe the displacement field: three translations (u,v,w), three rotations (the Euler angles α,β,γ), and the warping degree of freedom δ. The strain vector Eq (35) depends on these seven functions and their first derivatives through the very nonlinear relationships of Eqs. (27), (21), (22), (23), and (17), but formally we can write $\epsilon = \epsilon(h)$, where

$$h^T = (u, u', v, v', w, w', \alpha, \alpha', \beta, \beta', \gamma, \gamma', \delta, \delta') \tag{36}$$

The strain energy can now be reduced to a quadratic expression by means of the quasilinearization procedure[12] about a known configuration of the beam noted $\bar{h}$:

$$\tfrac{1}{2}\epsilon^T H \epsilon \approx \tfrac{1}{2}\bar{\epsilon} H \bar{\epsilon}^T + G^T(h-\bar{h}) + \tfrac{1}{2}(h-\bar{h})J(h-\bar{h}) \tag{37}$$

where

$$G_i = \bar{\epsilon}^T H \bar{\epsilon}_{,i}$$

$$J_{ij} = \bar{\epsilon}^T{}_{,i} H \bar{\epsilon}_{,j} + \bar{\epsilon}^T H \bar{\epsilon}_{,ij} \tag{38}$$

are the components of the equivalent load vector G and the tangent stiffness matrix J respectively. The notation $\bar{\epsilon}_{,i}$ means the derivative of the strain vector with respect to the ith function in h. This quadratic approximation to the strain energy can now be introduced into the Principle of Virtual Work, Eq. (34). The resulting expression provides a suitable basis for a finite-element approximation of the problem. Four-noded beam elements were found to be computationally efficient. At each node there are seven degrees of freedom corresponding to the seven displacements $u,v,w,\alpha,\beta,\gamma,\delta$. The solution of nonlinear problems is found iteratively by solving linearized equations about successive configurations of the beam.

Dynamic Analysis

In the analysis of flexible spinning beams such as helicopter blades, the natural frequencies of the structure about a nonlinear equilibrium position are of great interest to the designer. Figure 4 depicts the inertial triad $\boldsymbol{e}_x, \boldsymbol{e}_y, \boldsymbol{e}_z$ and the triad $\hat{\boldsymbol{e}}_x, \hat{\boldsymbol{e}}_y, \hat{\boldsymbol{e}}_z$ rotating with the blade at an angular velocity Ω about $\boldsymbol{e}_z$. The transformation matrix relating the base vector to the rotating triad is a known function of s

$$\begin{bmatrix} \lambda \\ \boldsymbol{i}_\xi \\ \boldsymbol{i}_\eta \end{bmatrix} = T(s) \begin{bmatrix} \hat{\boldsymbol{e}}_x \\ \hat{\boldsymbol{e}}_y \\ \hat{\boldsymbol{e}}_z \end{bmatrix} \tag{39}$$

The time derivatives of the base vectors are found as

$$\frac{\mathrm{d}}{\mathrm{d}t}\begin{bmatrix} \lambda \\ \boldsymbol{i}_\xi \\ \boldsymbol{i}_\eta \end{bmatrix} = \Omega T(s) \begin{bmatrix} 0 & 1 & 0 \\ -1 & 0 & 0 \\ 0 & 0 & 0 \end{bmatrix}$$

$$\times T^T(s) \begin{bmatrix} \lambda \\ \boldsymbol{i}_\xi \\ \boldsymbol{i}_\eta \end{bmatrix} = \Omega\bar{\Omega} \begin{bmatrix} \lambda \\ \boldsymbol{i}_\xi \\ \boldsymbol{i}_\eta \end{bmatrix} \tag{40}$$

where $\bar{\Omega}$ is a skew symmetric matrix. We can now express the position vector of a point $\boldsymbol{P}$ as

$$\boldsymbol{R} = \boldsymbol{r} + \bar{\boldsymbol{u}} + \tilde{\boldsymbol{u}} \tag{41}$$

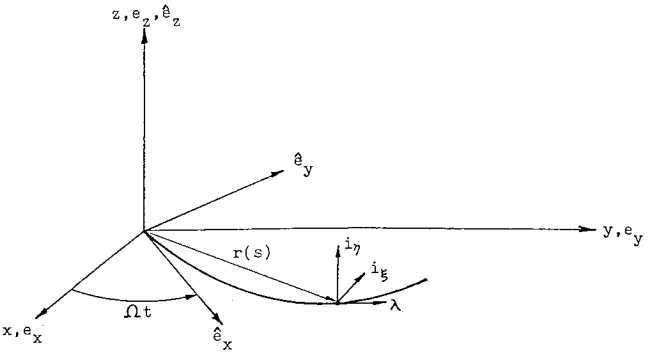

Fig. 4 Geometry of the rotating blade.

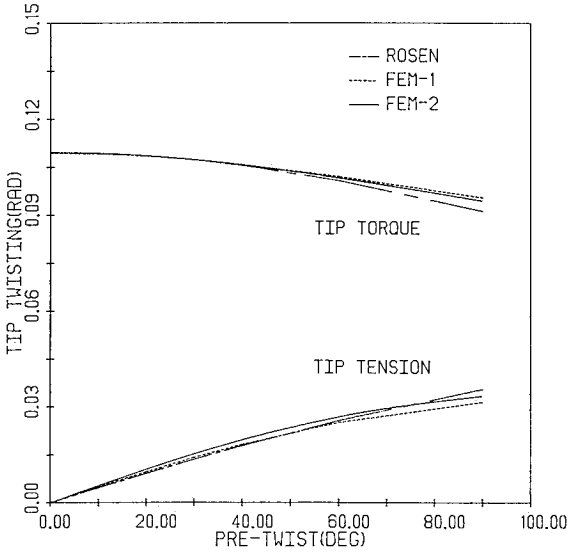

Fig. 5 Tip twist vs pretwist angle for a rectangular box beam under tip torque and tip tension.

where $\bar{u}$ is the known, steady equilibrium position of the spinning blade and $\tilde{u}$ a small, time-dependent perturbation about that equilibrium position. This can be written as

$$\boldsymbol{R} = [\lambda\ \boldsymbol{i}_\xi\ \boldsymbol{i}_\eta] \begin{bmatrix} \bar{U}+\tilde{U} \\ \bar{V}+\tilde{V} \\ \bar{W}+\tilde{W} \end{bmatrix} \tag{42}$$

where $\bar{U},\bar{V},\bar{W}$ are the components of $\boldsymbol{r}+\bar{\boldsymbol{u}}$ and $\tilde{U},\tilde{V},\tilde{W}$ the components of $\tilde{u}$, both expressed in the base vector triad. The inertia forces $\boldsymbol{F}_I$ are now readily calculated as the density distribution ρ multiplied by the second time derivative of the position vector $\boldsymbol{R}$, yielding

$$\boldsymbol{F}_I = -\rho\Omega^2 [\lambda\ \boldsymbol{i}_\xi\ \boldsymbol{i}_\eta] \left\{ \begin{bmatrix} \ddot{\tilde{U}} \\ \ddot{\tilde{V}} \\ \ddot{\tilde{W}} \end{bmatrix} + 2\bar{\Omega}^T \begin{bmatrix} \dot{\tilde{U}} \\ \dot{\tilde{V}} \\ \dot{\tilde{W}} \end{bmatrix} \right.$$

$$\left. + \bar{\Omega}^{2T} \begin{bmatrix} \tilde{U} \\ \tilde{V} \\ \tilde{W} \end{bmatrix} + \bar{\Omega}^{2T} \begin{bmatrix} \bar{U} \\ \bar{V} \\ \bar{W} \end{bmatrix} \right\} \tag{43}$$

These inertia forces can be treated with standard finite-element techniques to yield the mass matrix, the gyroscopic

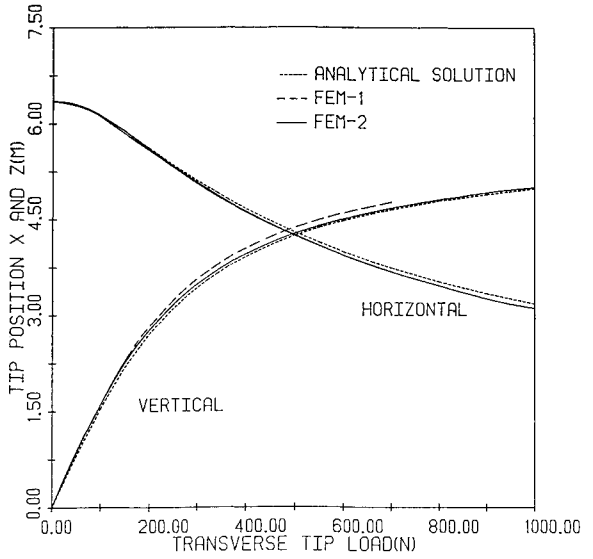

Fig. 6 Vertical and horizontal displacements of a rectangular box beam under tip transverse load.

matrix, the centrifugal stiffness matrix, and the centrifugal load vector corresponding to the four terms in Eq. (43) respectively. The natural vibration frequencies are the solutions of a quadratic eigenproblem that was solved with the Lanczos algorithm.[13]

Numerical Results

The behavior of the analysis will now be illustrated with several examples. In each case, the present analysis (referred to as FEM-2) will be compared with analytical or experimental solutions whenever available, and with a three-dimensional beam finite-element analysis (referred to as FEM-1) described in Ref. 6.

The results of the present analysis for static problems will be described first. The torsional behavior of a naturally twisted rectangular box beam under tip torque and axial load is analyzed in the first example. Figure 5 shows the tip twist of the beam as a function of the pretwisting angle. Note the torsional stiffening under tip torque and the "untwisting" under tip tension. In both cases, an excellent correlation is found between the two finite-element approaches and an analytical solution from Rosen.[14]

In the second example, the transverse displacements of a straight, rectangular box beam under tip transverse load is considered. Figure 6 shows the vertical and horizontal displacement at the tip of the beam vs the applied load. Note that the analysis was carried out to very large displacements and rotations (vertical displacement up to 5 m for a beam span of 6.35 m), yet both FEM analyses are in excellent correlation with the analytical solution.[15]

The last static example is a more involved analysis where the FEM results are compared with experimental measurements by Dowell and Traybar.[16] A slender beam with a solid aluminum rectangular cross section is subjected to a tip load P. The angle ϕ_0 between the loading direction and the major axis of the cross section (the "loading angle") can be varied from 0–90 deg in the experimental setup, yielding a wide range of nonlinear problems where torsion and bending are coupled. Figures 7a–7c show the tip twist angle, the flatwise tip displacement, and the edgewise tip displacement respectively vs the loading angle for three values of the tip load ($P=1$, 2, and 3 lb). In all cases, an excellent correlation is found between both FEM approaches and the experimental results.

We now turn to dynamic applications: the natural vibration frequencies ω of a uniform beam rotating at a constant

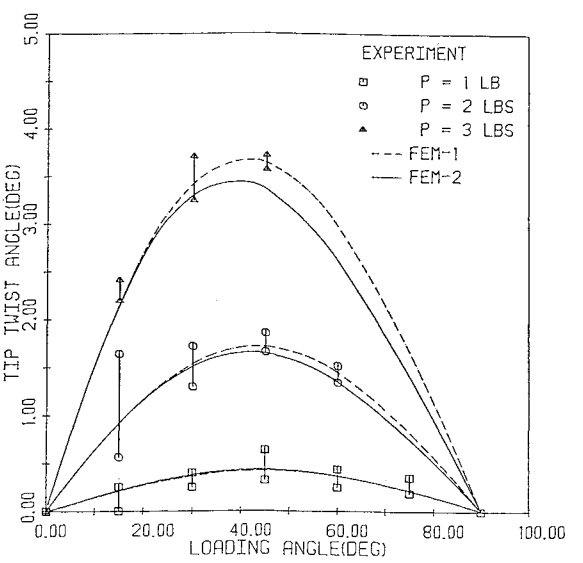

Fig. 7a Tip twist angle vs loading angle.

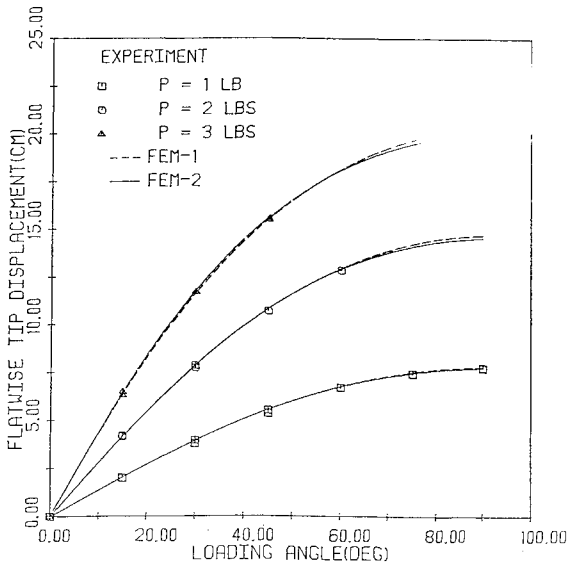

Fig. 7b Flatwise tip displacement vs loading angle.

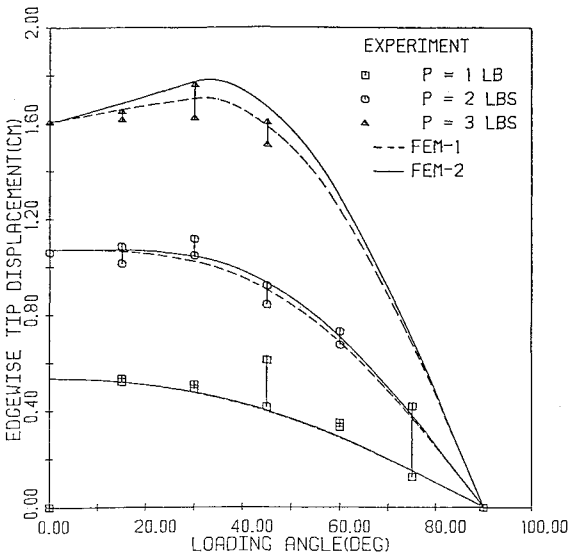

Fig. 7c Edgewise tip displacement vs loading angle.

Table 1 Dimensionless frequencies μ vs dimensionless angular speed λ

λ	First flapping mode		First lead-lag mode	
	Present	Reference 17	Present	Reference 17
0	3.516	3.516	3.516	3.516
2	4.138	4.137	3.621	3.622
4	5.585	5.585	3.895	3.898
6	7.360	7.360	4.258	4.263
8	9.257	9.257	4.647	4.657
10	11.20	11.20	5.033	5.049
12	13.17	13.17	5.403	5.427

Table 2 CPU time comparison for the various problems (in seconds)

Problem	FEM-1	FEM-2	Ratio
Pretwisted beam in torsion (linear)	0.8	0.2	4.0
Cantilevered beam deflection (nonlinear)	96.4	6.1	16.0
Cantilevered beam[16] $\phi_0 = 45$ deg (nonlinear)	57.4	2.2	25.0
Rotating beam frequencies (linear)	41.3	7.0	6.0

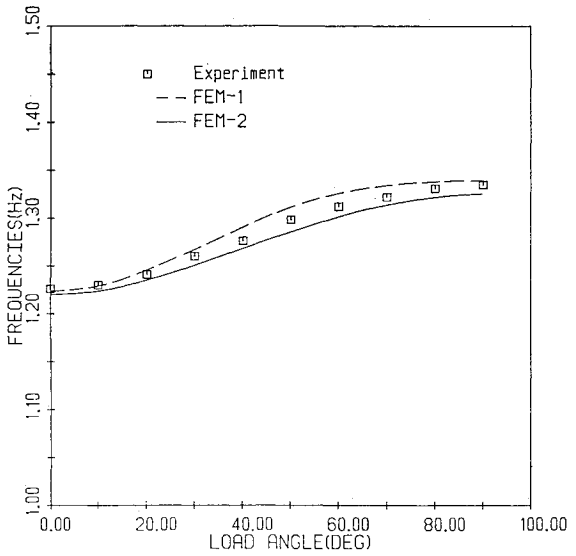

Fig. 8a Flapping frequency vs loading angle.

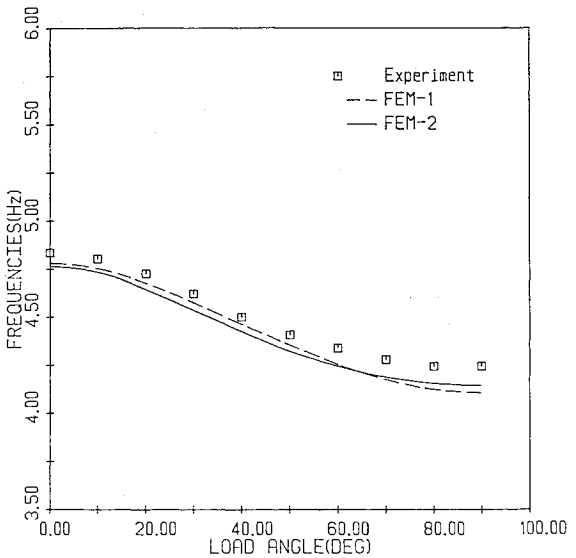

Fig. 8b Lead-lag frequency vs loading angle.

angular speed Ω about an axis fixed in space is analyzed first. Table 1 lists the dimensionless natural frequencies μ vs the dimensionless angular speed λ defined as

$$\mu = \omega\sqrt{\frac{mL^4}{EI}} \qquad \lambda = \Omega\sqrt{\frac{mL^4}{EI}}$$

where m is the mass per unit span, EI the bending stiffness, and L the span of the beam. The flapping frequencies are found to be in excellent agreement with the exact reference solution.[17] The agreement of the lead-lag frequencies is good, but for very high angular speed, slightly lower frequencies are predicted by the present solution, as it takes into account the elongation of the beam under centrifugal loading whereas the reference solution assumes an inextensible beam.

The experimental results of Dowell and Traybar[16] described in a previous paragraph also deal with the frequency measurements of small vibrations about a steady equilibrium position obtained by hanging a dead weight P at the tip of the beam. Both flapping and lead-lag frequencies are measured for various settings of the loading angle and are plotted in Figs. 8a and 8b respectively, together with the FEM predictions. Here again, theoretical results are in close agreement with experimental data.

In all the examples, the two finite-element approaches were found to correlate very closely; however, there is a significant difference in the computational effort involved in both methods. Table 2 summarizes the CPU times required by both FEM approaches in the various examples. In all cases, three four-noded elements were used, as this provides excellent accuracy. The present approach appears to be five times faster than three-dimensional beam elements for linear problems, and in nonlinear problems it is up to 20 times faster. This very significant improvement comes from a drastic reduction in the number of iterations probably due to a better modeling of the kinematics, particularly large rotations, and from the fivefold cost reduction of each linear step.

Conclusions

A finite-element approach to the large displacement analysis of naturally curved and twisted beams has been proposed and applied to both static and dynamic problems. The highlights of the method are as follows:

1) All the geometric nonlinearities are accurately accounted for, and the large rotations are represented by Euler angles.

2) The complex structural behavior of composite beams is modeled accurately as the following features are included: shearing deformations and torsion-related warping, arbitrary thin-walled cross sections, material anisotropy, and elastic couplings.

3) An excellent correlation with the analytical and experimental results has been demonstrated, even for very large deflections and rotations.

4) The computational cost has been drastically reduced as compared with other available formulations.

Appendix

The nonzero terms in the stiffness matrix H are as follows:

$$H(1,1) = \int_C A_{nn}\,d\zeta; \qquad H(1,2) = \int_C A_{nq}G_\xi\,d\zeta$$

$$H(1,3) = \int_C A_{nq}G_\eta\,d\zeta; \qquad H(1,4) = \int_C A_{nn}\xi\,d\zeta$$

$$H(1,5) = \int_C A_{nn}\eta\,d\zeta; \qquad H(1,6) = -\int_C A_{nq}r\,d\zeta$$

$$H(1,7)=\int_C (A_{nn}\tilde{\phi}+A_{nq}\bar{\phi})\mathrm{d}\zeta; \qquad H(1,8)=\int_C A_{nn}\phi\mathrm{d}\zeta$$

$$H(2,2)=\int_C A_{qq}G_\xi^2\mathrm{d}\zeta; \qquad H(2,3)=\int_C A_{qq}G_\xi G_\eta\mathrm{d}\zeta$$

$$H(2,4)=\int_C A_{nq}\xi G_\xi\mathrm{d}\zeta; \qquad H(2,5)=\int_C A_{nq}\eta G_\xi\mathrm{d}\zeta$$

$$H(2,6)=-\int_C A_{qq}rG_\xi\mathrm{d}\zeta$$

$$H(2,7)=\int_C (A_{qq}\bar{\phi}+A_{nq}\tilde{\phi})G_\xi\mathrm{d}\zeta$$

$$H(2,8)=\int_C A_{nq}\phi G_\xi\mathrm{d}\zeta$$

$$H(3,3)=\int_C A_{qq}G_\eta^2\mathrm{d}\zeta; \qquad H(3,4)=\int_C A_{nq}\xi G_\eta\mathrm{d}\zeta$$

$$H(3,5)=\int_C A_{nq}\eta G_\eta\mathrm{d}\zeta; \qquad H(3,6)=-\int_C A_{qq}rG_\eta\mathrm{d}\zeta$$

$$H(3,7)=\int_C (A_{qq}\bar{\phi}+A_{nq}\tilde{\phi})G_\eta\mathrm{d}\zeta; \qquad H(3,8)=\int_C A_{nq}\phi G_\eta\mathrm{d}\zeta$$

$$H(4,4)=\int_C A_{nn}\xi^2\mathrm{d}\zeta; \qquad H(4,5)=\int_C A_{nn}\xi\eta\mathrm{d}\zeta$$

$$H(4,6)=-\int_C A_{nq}\xi r\mathrm{d}\zeta; \qquad H(4,7)=\int_C (A_{nn}\tilde{\phi}+A_{nq}\bar{\phi})\xi\mathrm{d}\zeta$$

$$H(5,5)=\int_C A_{nn}\eta^2\mathrm{d}\zeta; \qquad H(5,6)=-\int_C A_{nq}\eta r\mathrm{d}\zeta$$

$$H(5,7)=\int_C (A_{nn}\tilde{\phi}+A_{nq}\bar{\phi})\eta\mathrm{d}\zeta$$

$$H(6,6)=\int_C A_{qq}r^2\mathrm{d}\zeta; \qquad H(6,7)=-\int_C (A_{qq}\bar{\phi}+A_{nq}\tilde{\phi})r\mathrm{d}\zeta$$

$$H(6,8)=-\int_C A_{nq}\phi r\mathrm{d}\zeta$$

$$H(7,7)=\int_C (A_{nn}\tilde{\phi}^2+A_{qq}\bar{\phi}^2+2A_{nq}\tilde{\phi}\bar{\phi})\mathrm{d}\zeta$$

$$H(7,8)=\int_C (A_{nn}\tilde{\phi}+A_{nq}\bar{\phi})\mathrm{d}\zeta$$

$$H(8,8)=\int_C A_{nn}\phi^2\mathrm{d}\zeta$$

Acknowledgments

This research was sponsored by the Army Research Office under Grant DAAG 29-82-K-0093. Dr. Robert Singleton is the contract monitor.

References

[1]Friedmann, P. P., "Recent Developments in Rotary-Wing Aeroelasticity," *Journal of Aircraft*, Vol. 14, Nov. 1977, pp. 1027–1041.

[2]Rosen, A. and Friedmann, P. P., "The Nonlinear Behavior of Elastic Slender Straight Beams Undergoing Small Strains and Moderate Rotations," *Journal of Applied Mechanics*, Vol. 46, March 1979, pp. 161–168.

[3]Mikulus, M. M. and Bush, H. G., "Advances in Structural Concepts, Large Space Antenna Systems Technology," NASA CP-2269, Pt. 1, May 1983, pp. 257–283.

[4]Bathe, K. J., *Finite Element Procedures in Engineering Analysis*, Prentice-Hall, Englewood Cliffs, NJ, 1982.

[5]Bathe, K. J., Almeida, C. A., and Ho., L. W., "A Simple and Effective Pipe Elbow Elements—Some Nonlinear Capabilities," *Computer and Structures*, Vol. 17, 1983, pp. 659–667.

[6]Bauchau, O. A. and Hong, C. H., "Finite Element Approach to Rotor Blade Modeling," *Journal of American Helicopter Society*, Vol. 32 (1), Jan. 1987, pp. 60–67.

[7]Washizu, K., *Variational Methods in Elasticity and Plasticity*, Pergamon Press, NY, 1975.

[8]Washizu, K., "Some Considerations on a Naturally Curved and Twisted Slender Beam," *Journal of Mathematics and Physics*, Vol. 48, No. 2, June 1964, pp. 111–116.

[9]Novozhilov, V. V., *Foundation of the Nonlinear Theory of Elasticity*, Graylock Press, Rochester, NY, 1953.

[10]Bauchau, O. A., "A Beam Theory for Anisotropic Materials," *Journal of Applied Mechanics*, Vol. 107, June 1985, pp. 416–422.

[11]Bauchau, O. A., Coffenberry, B. S., and Rehfield, L. W., "Composite Box Beam Analysis: Theory and Experiments," *Journal of Reinforced Plastics and Composites*, Vol. 7, Jan. 1987, pp. 25–35.

[12]Bellman, R. E. and Kalaba, R. E., *Quasilinearization and Non-Linear Boundary Value Problems*, American Elsevier Publishing Co., New York, 1965.

[13]Bauchau, O. A., "A Solution of the Eigen Problem for Undamped Gyroscopic Systems with the Lanczos Algorithm," *International Journal of Numerical Method Engineering*, Vol. 29, 1986, pp. 1–9.

[14]Rosen, A., "The Effect of Initial Twist on the Torsional Rigidity of Beams—Another Point of View," *Journal of Applied Mechanics*, Vol. 47, 1980, pp. 389–392.

[15]Holden, J. T., "On the Finite Deflection of Thin Beams," *International Journal of Solids and Structures*, Vol. 8, 1972, pp. 1051–1055.

[16]Dowell, E. H. and Traybar, J. J., "An Experimental Study of the Non-Linear Stiffness of a Rotor Blade Undergoing Flap, Lag, and Twist Deformations," Princeton Univ., Aerospace and Mechanical Science Rept. 1257, Dec. 1975.

[17]Hodges, D. H. and Rutkowski, M. J., "Free Vibration Analysis of Rotating Beams by a Variable-Order Finite Element Method," *AIAA Journal*, Vol. 19, Nov. 1981, pp. 1459–1466.